

# Heh2/Man1 may be an evolutionarily conserved sensor of NPC assembly state

Sapan Borah<sup>a</sup>, David J. Thaller<sup>a</sup>, Zhanna Hakhverdyan<sup>b</sup>, Elisa C. Rodriguez<sup>a</sup>, Anthony W. Isenhour<sup>a</sup>, Michael P. Rout<sup>b</sup>, Megan C. King<sup>a</sup>, and C. Patrick Lusk<sup>a,\*</sup>

<sup>a</sup>Department of Cell Biology, Yale School of Medicine, New Haven, CT 06520; <sup>b</sup>The Rockefeller University, New York, NY 10065

**ABSTRACT** Integral membrane proteins of the Lap2-emerin-MAN1 (LEM) family have emerged as important components of the inner nuclear membrane (INM) required for the functional and physical integrity of the nuclear envelope. However, like many INM proteins, there is limited understanding of the biochemical interaction networks that enable LEM protein function. Here, we show that Heh2/Man1 can interact with major scaffold components of the nuclear pore complex (NPC), specifically the inner ring complex (IRC), in evolutionarily distant yeasts. Although an N-terminal domain is required for Heh2 targeting to the INM, we demonstrate that more stable interactions with the NPC are mediated by a C-terminal winged helix (WH) domain, thus decoupling INM targeting and NPC binding. Inhibiting Heh2's interactions with the NPC by deletion of the Heh2 WH domain leads to NPC clustering. Interestingly, Heh2's association with NPCs can also be disrupted by knocking out several outer ring nucleoporins. Thus, Heh2's interaction with NPCs depends on the structural integrity of both major NPC scaffold complexes. We propose a model in which Heh2 acts as a sensor of NPC assembly state, which may be important for NPC quality control mechanisms and the segregation of NPCs during cell division.

## Monitoring Editor

Karsten Weis  
ETH Zurich

Received: Sep 10, 2020

Revised: Mar 22, 2021

Accepted: May 14, 2021

## INTRODUCTION

The eukaryotic genome is enclosed by a nuclear envelope that is contiguous with the endoplasmic reticulum (ER). Despite this continuity, the nuclear envelope contains a unique proteome that defines its function as a selective barrier. This barrier not only establishes nucleocytoplasmic compartmentalization but also directly impacts genome organization and function at the nuclear periphery (Mekhail

and Moazed, 2010; Taddei and Gasser, 2012; Buchwalter *et al.*, 2019). The key elements of this biochemical specialization are the nuclear pore complexes (NPCs), which control nucleocytoplasmic molecular exchange, and proteins specifically associated with the inner and outer nuclear membranes (INM and ONM) (Ungricht and Kutay, 2017; Hampoelz *et al.*, 2019). While ONM proteins generally act as adaptors that connect the cytoskeleton to the nucleus (Burke and Roux, 2009), INM protein function is less well defined. This is due in part to challenges inherent with defining biochemical interactions between low-abundance integral membrane proteins that exist within a complex and integrated network of peripheral chromatin and nuclear scaffold proteins like the lamins (outside of yeasts). Nonetheless, there is confidence that there are several dozen integral INM proteins with the most evolutionarily conserved families being the LAP2-emerin-MAN1 (LEM) and the Sad1, UNC-84 (SUN) proteins (Mans *et al.*, 2004; Ungricht and Kutay, 2015).

LEM family proteins are so named for their LEM domain, a short ~40-amino-acid helix-extension-helix motif that, at least in metazoa, binds to barrier to autointegration factor (BAF) (Furukawa, 1999; Cai *et al.*, 2007). As there is no BAF in yeasts, their LEM domain containing proteins must possess other conserved functions, which may more directly relate to genome integrity, ensuring the stability of repetitive DNA (Mekhail *et al.*, 2008) and also contributing to the

This article was published online ahead of print in MBoc in Press (<http://www.molbiolcell.org/cgi/doi/10.1091/mbc.E20-09-0584>) on May 19, 2021.

\*Address correspondence to: C. Patrick Lusk ([patrick.lusk@yale.edu](mailto:patrick.lusk@yale.edu)).

Abbreviations used: a.u., arbitrary unit; BAF, barrier to autointegration factor; CV, coefficient of variation; ER, endoplasmic reticulum; FKBP12, FK506 binding protein; FRB, FKBP12 rapamycin bindin; GFP, green fluorescent protein; IDR, intrinsically disordered region; IgG, immunoglobulin G; INM, inner nuclear membrane; IRC, inner ring complex; LD, luminal domain; LEM, Lap2-emerin-MAN1; MS, mass spectrometry; NLS, nuclear localization signal; NPC, nuclear pore complex; nup, nucleoporin; ONM, outer nuclear membrane; ORC, outer ring complex; Sc, *Saccharomyces cerevisiae*; SD, standard deviation; SDS-PAGE, sodium dodecyl sulphate-polyacrylamide gel electrophoresis; Sp, *Schizosaccharomyces pombe*; SUN, Sad1, UNC-84; TAP, tandem affinity purification; TM, transmembrane; WH, winged helix; WT, wild type.

© 2021 Borah *et al.* This article is distributed by The American Society for Cell Biology under license from the author(s). Two months after publication it is available to the public under an Attribution-Noncommercial-Share Alike 3.0 Unported Creative Commons License (<http://creativecommons.org/licenses/by-nc-sa/3.0>).

"ASCB®," "The American Society for Cell Biology®," and "Molecular Biology of the Cell®" are registered trademarks of The American Society for Cell Biology.

mechanical integrity of the nucleus (Schreiner *et al.*, 2015). There are up to seven LEM domain proteins in humans but in the two most commonly used yeast models, *Saccharomyces cerevisiae* (Sc) and *Schizosaccharomyces pombe* (Sp) there are only two: ScHeh1(Src1)/SpHeh1(Lem2) and ScHeh2/SpHeh2(Man1) (Barton *et al.*, 2015). Of these two, ScHeh1 and SpHeh1 are likely orthologues derived from a common ancestor, while ScHeh2 and SpHeh2 resulted from independent duplication events of their respective paralogues ScHeh1 and SpHeh1 (Rhind *et al.*, 2011; Gonzalez *et al.*, 2012). Despite their independent evolutionary history, there is evidence that Heh2 in both yeasts specifically makes functional connections with NPCs. For example, in *S. cerevisiae*, we demonstrated synthetic genetic interactions between genes encoding NPC components (nucleoporins or nups), and *HEH2* (Yewdell *et al.*, 2011). In the *S. pombe* cousin *Schizosaccharomyces japonicus*, it has also been suggested that Heh2 supports connections between chromatin and NPCs to enable their segregation between daughter cells in mitosis (Yam *et al.*, 2013). However, the underlying biochemical connections between Heh2 and the NPC are not understood.

Understanding the nature of the connections between Heh2 and NPCs may also help illuminate mechanisms underlying the biogenesis of NPCs. As the total proteome, interactome, and structure of NPCs have come to light, it is now understood that the enormous (50–100 MD) NPC is built from a relatively small (~30) number of nups (Hampoelz *et al.*, 2019; Fernandez-Martinez and Rout, 2021). These nups are organized into modular subcomplexes that, in multiples of eight, assemble the eightfold radially symmetric NPC scaffold composed of inner and outer ring complexes (IRC and ORC), a coaxial membrane ring complex, the central transport channel, and asymmetric (perpendicular to the plane of the nuclear envelope) mRNA export platform and nuclear basket (Kosinski *et al.*, 2016; Kim *et al.*, 2018). How NPCs are assembled in space and time during interphase remains ill-defined but likely begins within the nucleus at the INM (Marelli *et al.*, 2001; Makio *et al.*, 2009; Yewdell *et al.*, 2011; Mészáros *et al.*, 2015; Otsuka *et al.*, 2016). The recruitment of nups to an assembly site occurs alongside membrane remodeling that evaginates the INM and ultimately drives fusion with the ONM (Otsuka *et al.*, 2016). Consistent with an inside-out model, the cytosolic-facing mRNA export platform is likely added at a terminal step in NPC assembly (Otsuka *et al.*, 2016; Onischenko *et al.*, 2017). In genetic backgrounds where the cytoplasmic-facing mRNA export platform is not assembled, herniations or blebs are observed over assembling NPCs, which may reflect defects in INM–ONM fusion and/or the triggering of NPC assembly quality control pathways (Thaller and Lusk, 2018; Thaller *et al.*, 2021).

Both Heh1 and Heh2 have been implicated in mechanisms of NPC assembly quality control in which they regulate the recruitment of the endosomal sorting complexes required for transport (ESCRT) to the nuclear envelope (Webster *et al.*, 2014, 2016; Thaller *et al.*, 2019). One early model suggested that Heh2 may differentially bind to NPC assembly intermediates over fully formed NPCs (Webster *et al.*, 2014). However, this has yet to be formally interrogated. To be more incisive as to how Heh2 impacts NPC function, here we have thoroughly analyzed the biochemical interaction network of endogenous Heh2. Using two evolutionarily distant yeasts, we show that Heh2 can copurify with the NPC's IRC. These interactions do not require the LEM domain or any INM targeting sequences but instead depend on a C-terminal domain predicted to fold into a winged helix (WH) (Caputo *et al.*, 2006). Further, by decoupling NPC clustering from perturbations to NPC structure, we demonstrate that Heh2 associates with NPCs *in vivo*. Most interestingly, the association of Heh2 with NPCs can be diminished by knocking out

components of the ORC. These data suggest that Heh2's interaction with the NPC depends on the latter's structural integrity. Taking the results together, we suggest a model in which Heh2 may be a sensor of NPC assembly state.

## RESULTS

### Heh2 binds to specific nups in evolutionarily distant yeasts

To better define the interacting partners of Heh1 and Heh2, we performed one-step affinity purifications of Heh1-TAP and Heh2-TAP (produced at endogenous levels) from cryolysates derived from logarithmically growing budding yeast (Hakhverdyan *et al.*, 2015). As shown in Figure 1A, we did not detect any obvious stoichiometric binding partners of Heh1-TAP despite robust recovery of the fusion protein. In marked contrast, Heh2-TAP copurified with at least eight additional proteins, which were visible by SDS–PAGE and Coomassie blue staining of bound fractions. Excision of these bands followed by mass spectrometric (MS) protein identification revealed that Heh2 interacts with the IRC of the NPC and a subset of cytosolic-facing nups, including Nup159, Nup188, Nup192, Nup170, Pom152, Nup157, Nup116, Nic96, and Nsp1 (Supplemental Table S1). For context, we have colored the identified nups in a diagram of a single spoke from the budding yeast NPC structure (Kim *et al.*, 2018) in Figure 1A.

We were next curious as to whether Heh2's interaction with nups was also observed in other yeast species where the NPC structure is different from that in budding yeast. For example, fission yeast NPCs are made up of a similar catalogue of nups (Baï *et al.*, 2004; Chen *et al.*, 2004; Asakawa *et al.*, 2014), but there is evidence that there is asymmetry with respect to the ORC, which contains 16 copies (instead of eight) of the “Y” complex on the nucleoplasmic side of the NPC (Asakawa *et al.*, 2019). Of additional interest, although *HEH1* in both *S. cerevisiae* and *S. pombe* is derived from a common ancestor, these yeasts are separated by ~500 million years of evolution (Rhind *et al.*, 2011). Intriguingly, and in contrast, *ScHEH2* and *SpHEH2* arose from distinct duplication events (Mans *et al.*, 2004) and might therefore be expected to carry out distinct functions.

Interestingly, however, despite this unique evolutionary history, the affinity purifications of SpHeh2-TAP and SpHeh1-TAP were qualitatively similar to those of the *S. cerevisiae* versions. For example, only SpHeh2-TAP copurified with several specific proteins (Figure 1B). Note that SpHeh2-TAP is proteolytically sensitive and is purified both as a full-length (~115 kDa) and a smaller (~65 kDa) form (Figure 1B). Nonetheless, like its distant *S. cerevisiae* cousin, the SpHeh2 complex consisted of essentially the same subset of inner ring nups including Nup184, Nup186, Nup155, Pom152, Npp106, Nup98, and Nup97 (Figure 1B; Supplemental Table S1). To facilitate a comparison, the *S. cerevisiae* homologues are listed next to the identified *S. pombe* nups in Figure 1B. Thus, despite the distinct duplication events that gave rise to *HEH2* in both species, the physical association of Heh2 with the IRC likely points to an important and conserved function that was likely shared by a common ancestor before being independently specialized in the two species lineages.

### Heh2 colocalizes with NPCs

The affinity purifications strongly suggested that Heh2 can interact with NPCs *in vivo*. To test whether this association could be observed in living cells by light microscopy, we took advantage of a NPC clustering strategy that leverages the Anchor Away approach (Haruki *et al.*, 2008). The latter relies on the rapamycin-mediated dimerization of FRB and FKBP12 protein domains. In prior work, we had observed that NPCs could be rapidly (within 15 min) clustered

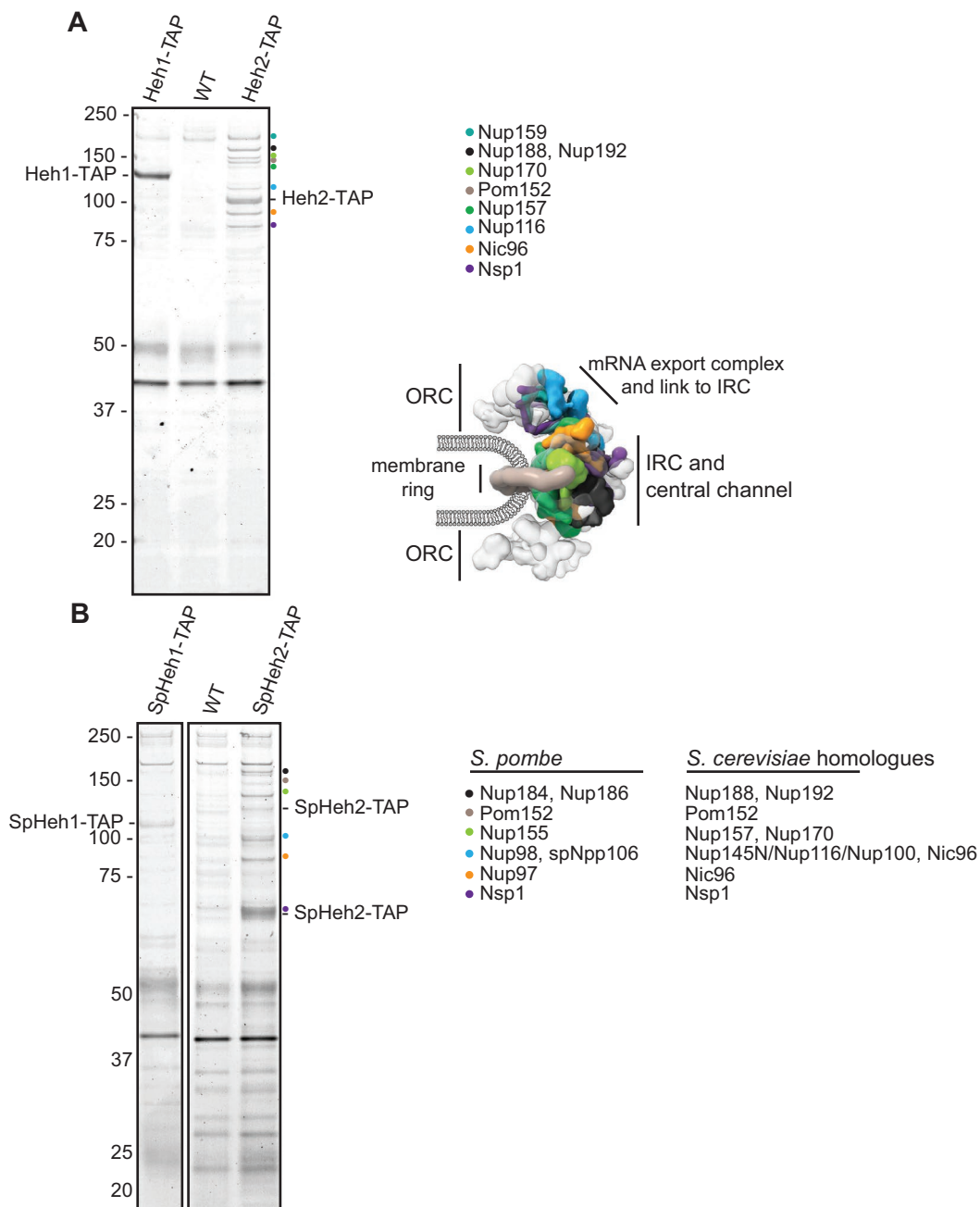


**FIGURE 1:** Heh2 binds to specific nups in evolutionary distant yeasts. (A) Heh2 specifically binds the IRC. Affinity purifications were performed from cell extracts derived from strains expressing endogenous Heh1-TAP or Heh2-TAP or from WT cells (no TAP). Bound proteins were separated by SDS-PAGE and visualized by Coomassie staining. Numbers at the left indicate positions of molecular weight standards in kilodaltons. Positions of Heh1-TAP and Heh2-TAP are indicated, and colored circles indicate proteins identified by MS from the Heh2-TAP lane, as indicated in the key (see Supplemental Table S1). This color scheme is also used to indicate positions of nups within a single spoke of the NPC structure (from PDBDEV\_00000010; Kim *et al.*, 2018). ORC is outer ring complex, IRC is inner ring complex. (B) As in A but affinity purifications performed from *S. pombe* cell extracts. The corresponding *S. cerevisiae* homologues of the identified *S. pombe* nups are also listed.

by treating cells expressing a NPC-incorporated Nsp1-FRB fusion and a plasma membrane Pma1-FKBP12 anchor with rapamycin (Figure 2A). The speed of clustering indicated that fully formed NPCs were driven into clusters independently of NPC misassembly. Further, we did not detect any removal of Nsp1-FRB from NPCs under these conditions (Colombi *et al.*, 2013). Consistent with this premise, we assessed the colocalization of Nup82-GFP with

Nup170-mCherry in strains expressing Nsp1-FRB and Pma1-FKBP12 in the presence of carrier alone (dimethyl sulfoxide [DMSO]) or rapamycin. As expected, both of the fluorescent proteins localized in a punctate distribution at the nuclear envelope in the presence of carrier only with a significant  $r = 0.48$  positive correlation between the green fluorescent protein (GFP) and mCherry fluorescence (Figure 2B, far right panel). Upon the addition of rapamycin, we

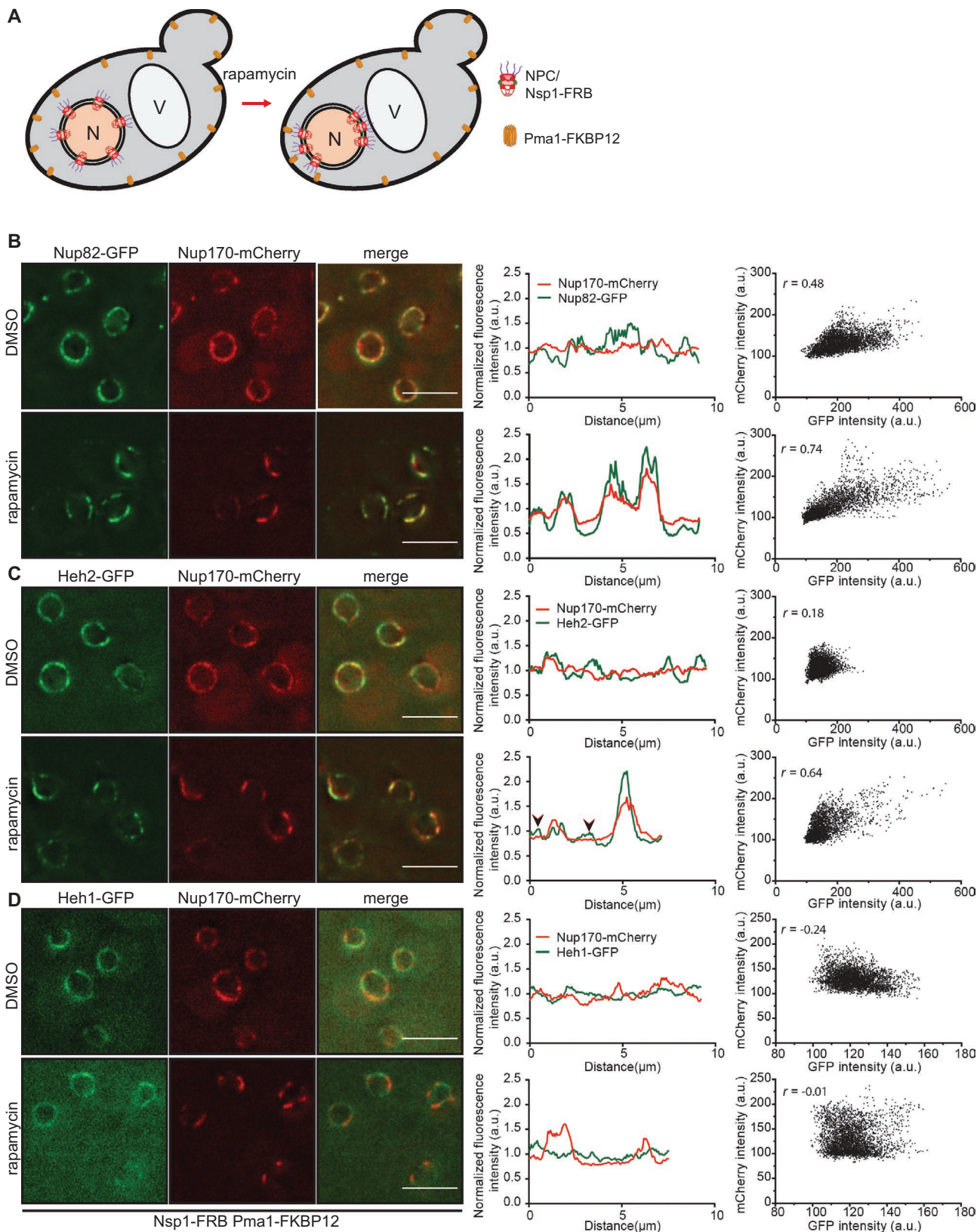


**FIGURE 2:** Heh2 associates with NPCs in vivo. (A) Schematic of NPC clustering assay mediated by the rapamycin-induced dimerization of Nsp1-FRB (at the NPC) and Pma1-FKBP12. N is nucleus, V is vacuole. (B–D) Left: Deconvolved fluorescence micrographs of indicated GFP-tagged proteins and Nup170-mCherry as a NPC marker with merge in cells treated with DMSO (carrier) or rapamycin for 30 min. Scale bar is 5  $\mu$ m. Middle: Line profiles of fluorescence intensity of GFP and mCherry fusions (in arbitrary units, a.u.) along the nuclear envelope of a single cell. Arrowheads indicate peaks of Heh2-GFP but not Nup170-mCherry. Right: Scatterplot with Pearson correlation coefficient ( $r$ ) of GFP and mCherry fluorescence intensity (in arbitrary units, a.u.) along the nuclear rim of 30 cells, from three independent experiments.

observed rapid clustering and concurrent colocalization of both signals along the nuclear envelope, which were evident in the coincidence of the GFP and mCherry fluorescence peaks of line profiles along the nuclear envelope and a correlation that increased to  $r = 0.74$  (Figure 2B, middle and right panels).

We next tested how this approach to NPC clustering influenced Heh2-GFP localization. As a control, we also assessed the distribution of Heh1-GFP, which does not detectably interact with nups (Figure 1A). As shown in Figure 2C, the addition of rapamycin led to the clear colocalization of Heh2-GFP and Nup170-mCherry. This again was evident through the examination of line profiles of a representative nuclear envelope where there was coincidence between the peaks of the GFP and mCherry fluorescence and was supported by the increased positive correlation of GFP and mCherry fluorescence (from  $r = 0.18$  to  $r = 0.64$ ; Figure 2C, middle and right panels). Note, however, that unlike the comparison between the two nups (Figure 2B), there are peaks of Heh2-GFP fluorescence that are not coincident with the NPC clusters (Figure 2C, arrowheads in line profiles). Thus, while it is clear that Heh2-GFP associates with NPCs, there is also an additional pool of Heh2-GFP at the INM. Last, we did not observe similar effects with Heh1-GFP, which failed to cluster with NPCs (Figure 2D) or correlate with their distribution ( $r = -0.01$ ) (Figure 2D, right panel). Thus, this NPC clustering approach faithfully mirrored the biochemical analysis of both Heh1 and Heh2 and supports the interpretation that Heh2 shares interactions with NPCs and the INM.

### Inhibition of NPC assembly reduces the Heh2 pool bound to NPCs

A model in which there are two pools of Heh2 was further supported by experiments where we reduced NPC number by inhibiting NPC assembly. For example, by again leveraging the Anchor Away strategy, we inhibited NPC assembly by trapping newly synthesized Nup192-FRB-GFP for 3 h (Colombi *et al.*, 2013). Under these conditions, there is a reduction in the number of NPCs that is reflected by lower levels of Nup192-FRB-GFP at the nuclear envelope and a concomitant accumulation of newly synthesized Nup192-FRB-GFP at the plasma membrane (Figure 3, A and B, rapamycin panels, arrows). In this scenario, we tested whether Nup192-FRB-GFP and Heh2-mCherry colocalized at the nuclear envelope (Figure 3B). As a control, we also tested colocalization with Pom152-mCherry (Figure 3A). Although Pom152-mCherry distribution was similar to that of Nup192-FRB-GFP with line profiles showing coincidence between mCherry and GFP fluorescence peaks along the nuclear envelope with correlation between GFP and mCherry fluorescence (Figure 3A, middle and right panels), there were gaps in the Nup192-FRB-GFP signal that were filled by Heh2-mCherry (Figure 3B, see arrowheads). This result was also represented in line profiles along the nuclear envelope where Heh2-mCherry fills areas that are devoid of GFP peaks and reduced correlation of GFP and mCherry signals (Figure 3B, middle and right bottom panels). Importantly, however, a subset of Nup192-FRB-GFP peaks that likely correspond to NPCs that were assembled before rapamycin addition still coincided with Heh2-mCherry peaks (Figure 3B, middle bottom panel). Thus, these data are consistent with the interpretation that inhibition of NPC assembly leads to a decrease in the pool of Heh2 bound to NPCs (due to their reduced number) and an increase in the free pool at the INM. This conclusion is further supported by affinity purifications of Heh2-TAP from Nup192-FRB-GFP strains under the same conditions. While in DMSO-treated conditions the expected IRC profile of nups was detected (Figure 3C), upon inhibition of NPC assembly with rapamycin, we observed an ~2–3-fold reduction in the number

of these nups (orange line in densitometry plot at right) while the total amount of Heh2-TAP affinity purified remained unchanged (Figure 3C). Importantly, we did not observe any changes to at least Pom152 total levels under these conditions (Figure 3D). Thus, we favor a model in which Heh2 remains capable of binding to the IRC in fully formed NPCs, even when their number is decreased upon assembly inhibition.

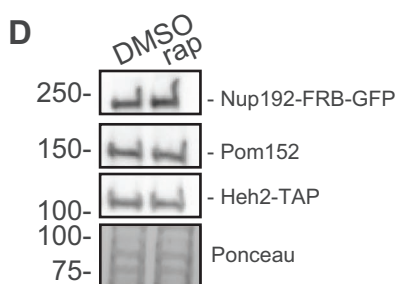
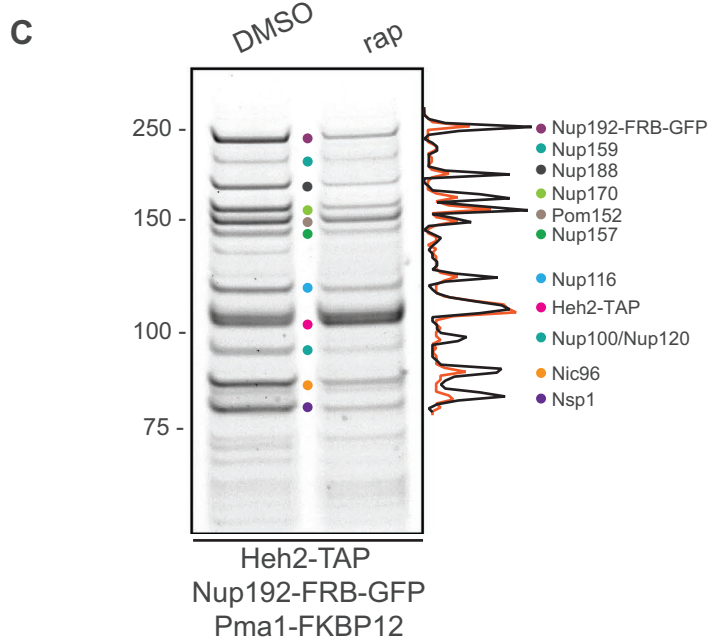
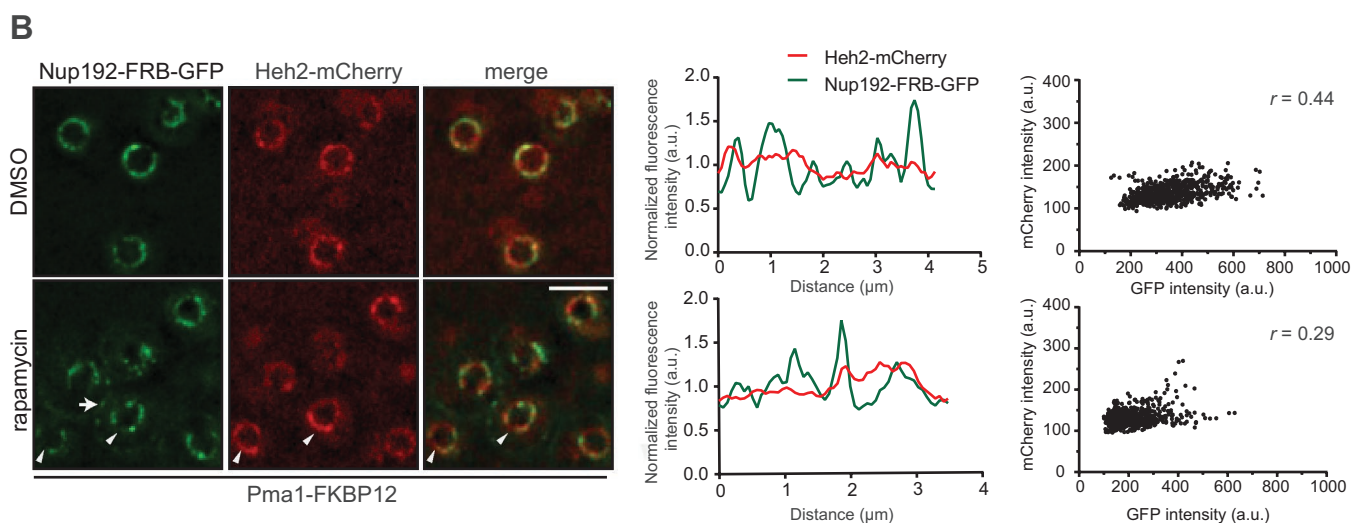
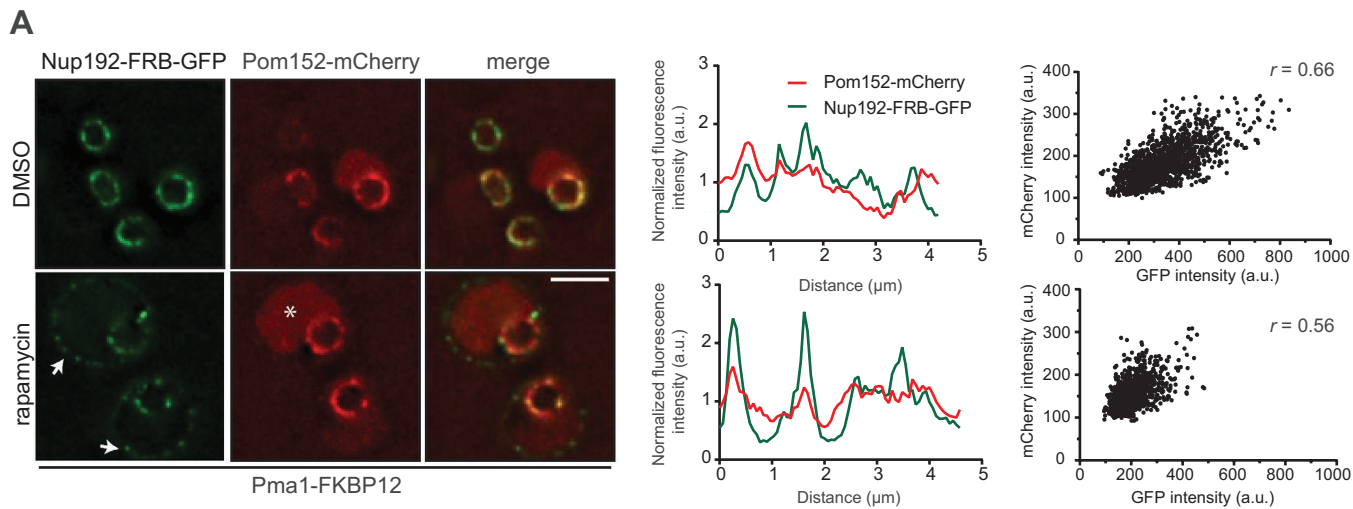
### Heh2's association with NPCs depends on the integrity of the NPC scaffold

We next explored the hierarchy of physical interactions that control Heh2's binding to the IRC by affinity purifying Heh2-TAP from several IRC nup deletion backgrounds. As a control, we also tested the impact of deletion of *NUP133*, which encodes a component of the ORC. Interestingly, we were unable to define any single knockout of an inner ring nup that fully disrupted Heh2's biochemical association with this complex. For example, in cases where we deleted the genes encoding Nup157 or Pom152, we observed the discrete loss of these, and only these, proteins from bound fractions (Figure 4, A and B). Deletion of *NUP170* and *NUP188* led to a more severe disruption of nups bound to Heh2, but in these cases, Pom152 and a band at the molecular weight of Nup159 remained (Figure 4, A and B). Thus, it seems likely that Heh2 makes several direct connections to nups in the IRC, with the most obvious candidates being Pom152, Nup170, and/or Nup188.

These data are also consistent with the lack of any major change to Heh2-GFP distribution in the *nup170Δ*, *nup188Δ*, and *pom152Δ* strains; in all cases the punctate, NPC-like distribution of Heh2-GFP was retained (Figure 4C, quantified in D). The one exception was that, in addition to the punctate nuclear envelope distribution, a cortical ER pool of Heh2-GFP could be discerned specifically in *nup170Δ* strains (Figure 4C, arrowhead). These data are consistent with prior work demonstrating that Nup170 is required for the efficient targeting of overexpressed Heh2 to the INM (King *et al.*, 2006). They further support a model in which the role of Nup170 in targeting Heh2 to the INM may be independent of its contribution to Heh2-IRC binding.

In striking contrast to the IRC nup deletions, the removal of the ORC nup Nup133 led to a virtually complete loss of binding between Heh2 and the IRC (Figure 4A). This was surprising as we did not detect any significant enrichment of ORC components in the affinity purifications of Heh2. Consistent with the functional relevance of this finding, we observed a similar loss of SpHeh2's interactions with nups upon deletion of the Nup133 homologue spNup132 (Figure 4E). We considered two scenarios to explain these data. First, it was possible that NPC clustering, which occurs in the absence of Nup133 (Doye *et al.*, 1994; Pemberton *et al.*, 1995), prevented Heh2 from binding to NPCs. Alternatively, it was possible that Heh2 reported on the integrity of the NPC scaffold, which is likely compromised without this key ORC component.

To begin to differentiate between these possibilities, we examined the distribution of Heh2-GFP in several genetic backgrounds where NPC clustering has been observed. We first tested colocalization between Heh2-GFP and Nup82-mCherry in a strain expressing the *nup159-1* temperature-sensitive allele (Gorsch *et al.*, 1995). This strain is particularly useful for this analysis as clustering of NPCs occurs at the permissive temperature for the *nup159-1* allele (i.e., room temperature) when NPCs are thought to be fully assembled. Consistent with this assertion, Nup82-mCherry is clustered at the nuclear envelope at room temperature (Figure 5A), whereas its colocalization at the nuclear envelope at the nonpermissive temperature (37°C) is diminished because it cannot be stably incorporated into



NPCs without a functional Nup159 (Supplemental Figure S1). Under the permissive NPC clustered condition, we observed the colocalization of Heh2-GFP and Nup82-mCherry (Figure 5A). In fact, we calculated that ~70% of the Heh2-GFP at the nuclear envelope was found colocalized with the clustered Nup82-mCherry, which was similar to, if not higher than, the proportion of Heh2 at NPCs using the Nsp1-FRB Anchor Away clustering approach (Figure 5B). Taking the data together, we conclude that NPC clustering per se does not impact Heh2's interaction with NPCs.

We therefore next explored how disrupting several components of the ORC contributed to Heh2-GFP's association with NPCs in vivo. Consistent with the interpretation that Heh2 requires a functional ORC to bind NPCs, the deletion of both *NUP84* and *NUP120* led to an obvious diminishment of the proportion of Heh2-GFP that colocalized with the clustered Nup82-mCherry in these strains (Figure 5, A and B). Most strikingly and consistent with the biochemical analysis, we observed a near complete loss of Heh2-GFP association with clustered NPCs in *nup133Δ* cells (Figure 5, A and B). In fact, there were often clear gaps in the Heh2-GFP signal at the nuclear envelope that corresponded to the location of the *nup133Δ* NPC clusters (Figure 5A, arrowheads). A similar result was observed in *Spnup132Δ* cells (Supplemental Figure S2). Thus, we conclude that Heh2 requires a functional ORC for its association with the NPC and might therefore be capable of sensing the integrity of the NPC scaffold.

### The conserved WH domain of Heh2 is required for NPC association

We next wished to determine the sequence elements of Heh2 that conferred binding to the NPC and whether they were distinct from those required for INM targeting. We therefore generated truncations of Heh2 where the N-terminal nucleoplasmic domain (which contains the INM-targeting information [King *et al.*, 2006; Meinema *et al.*, 2011]) and the C-terminal WH domains are deleted (Figure 6A). Interestingly, deletion of the N-terminus did not impact binding to nups, as a similar (if more robust) profile of the IRC was recovered in affinity purifications of *heh2-(316-663)*-TAP (Figure 6B). These data suggest that Heh2 can reach the NPC (or at least bind to nups) in the absence of its N-terminal INM targeting domain. In marked contrast, deletion of the WH domain, which does not impact INM

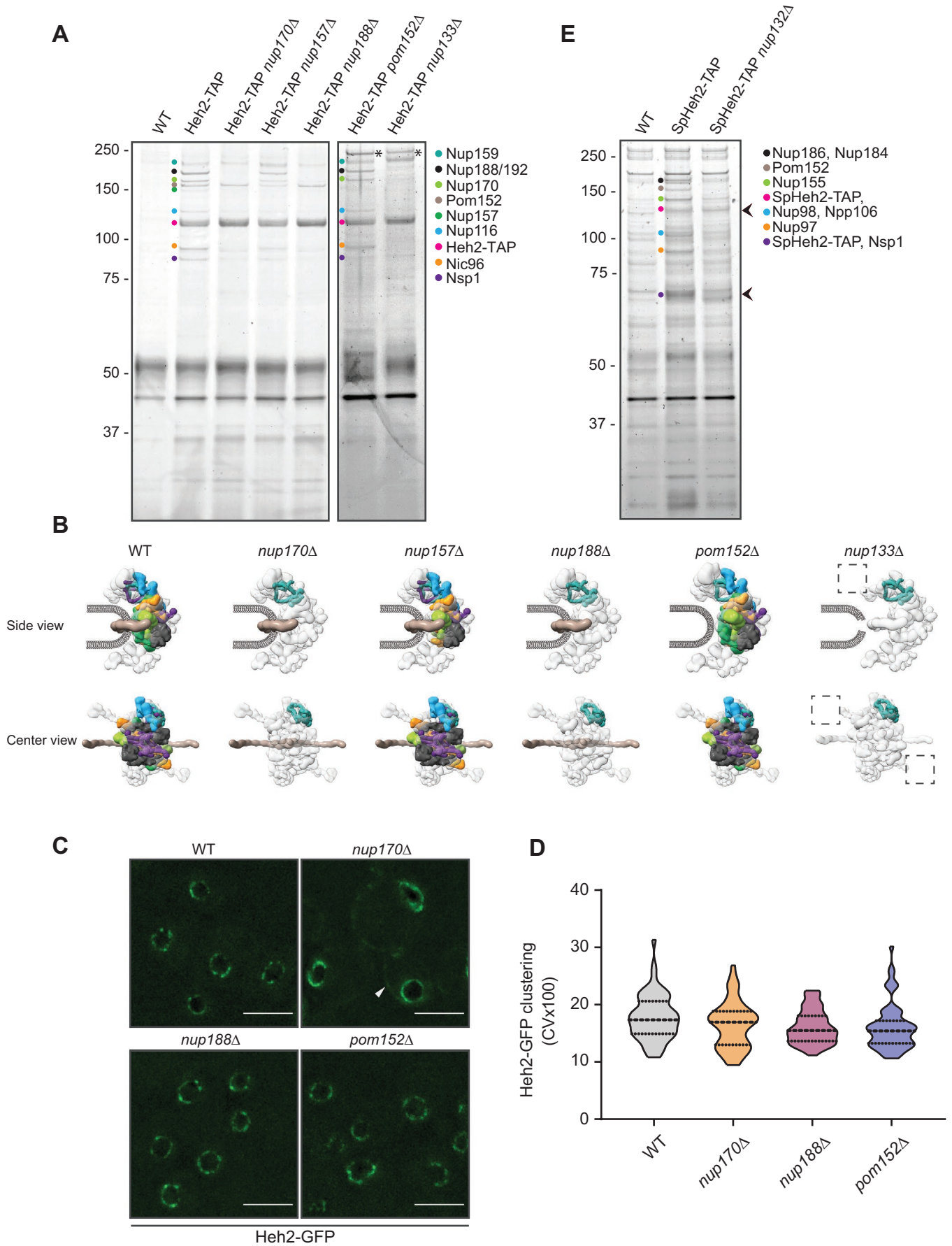
targeting (Meinema *et al.*, 2011), led to a striking reduction of nup binding (Figure 6B). These results were also mirrored in vivo. For example, compared with Heh2-GFP, *heh2-(1-570)*-GFP did not exhibit a punctate distribution at the nuclear envelope (Figure 6C), which was quantified as a reduced coefficient of variation (CV) of the fluorescence signal along the nuclear envelope (Figure 6D). Consistent with the idea that this change in localization of *heh2-(1-570)*-GFP was due to a loss of its interaction with NPCs, it also failed to cluster with NPCs in the Nsp1-FRB Anchor Away NPC clustering assay (Figure 6E) with no positive correlation between *heh2-(1-570)*-GFP and Nup170-mCherry signals in either DMSO ( $r = 0.0$ ) or rapamycin ( $r = -0.08$ )-treated cells (Figure 6F). Thus, the WH domain of Heh2 is required for stable binding to NPCs.

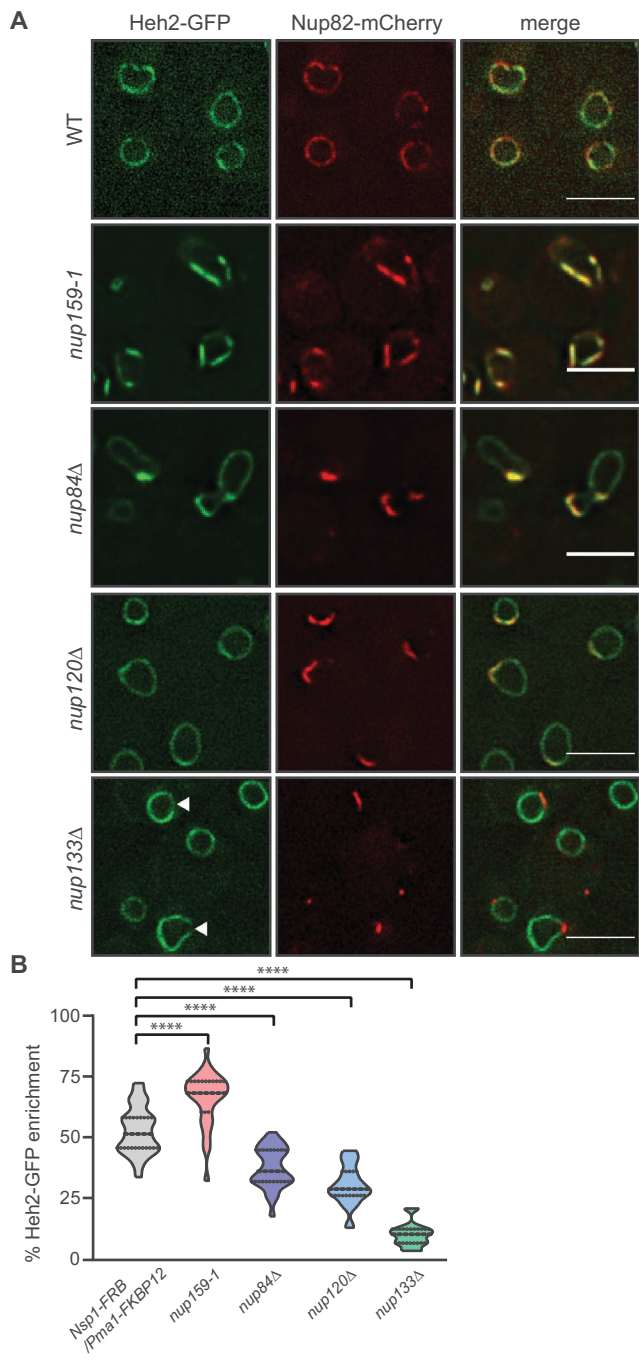
### WH-domain-mediated interactions with NPCs are required for normal NPC distribution

As the Heh2 WH domain was specifically required for Heh2 binding to NPCs, but not for INM targeting, there was an opportunity to define a putative NPC-specific function for Heh2. Indeed, deletion of *HEH2* leads to a marked clustering of Nup82-GFP, which was quantified as a CV of the fluorescence along the nuclear envelope that was approximately double the value in wild-type (WT) cells (Figure 6, G and H). To directly test whether this phenotype was due to a loss of nup binding, we assessed the distribution of Nup82-GFP in cells expressing *heh2-(1-570)*. Indeed, as shown in Figure 6G, this targeted abrogation of the nup-binding WH domain also resulted in a clear redistribution of Nup82-GFP, showing a clustering coefficient nearly identical to that seen in *heh2Δ* cells (Figure 6H). Thus, interactions between Heh2 and the NPC are required for normal NPC distribution.

Interestingly, expression of *heh2-(316-663)* from its endogenous locus also impacted NPC distribution, but with a unique phenotype. Because this truncation of Heh2 lacks its INM targeting information, this fusion will be mislocalized to the ER (King *et al.*, 2006; Meinema *et al.*, 2011). In these cells, Nup84-GFP accumulated in clusters at the nuclear envelope but also appeared within cytosolic foci (Figure 6I, arrowheads) in ~17% of cells (Figure 6J). Together then, these data support a model in which both the N-terminal and C-terminal domains of Heh2 are important for NPC distribution; however, the underlying mechanisms behind these alterations are unique and

**FIGURE 3:** Inhibition of NPC assembly reduces the Heh2-nup bound pool. (A, B) Left: Deconvolved fluorescence micrographs of Nup192-FRB-GFP with either Pom152-mCherry or Heh2-mCherry with merge after cells were treated with DMSO (carrier) or rapamycin for 3 h to inhibit NPC assembly. Note accumulation of newly synthesized Nup192-FRB-GFP at the plasma membrane as it binds to the Pma1-FKBP12 anchor indicated by arrows. The asterisk denotes vacuolar autofluorescence. Arrowheads point to areas where Heh2-mCherry does not colocalize with Nup192-FRB-GFP. Scale bar is 2  $\mu$ m. Middle: Line profiles of GFP and mCherry fluorescence intensity (in arbitrary units, a.u.) along the nuclear envelope of single cells corresponding to DMSO (top) and rapamycin (bottom) conditions. Right: Scatterplot with Pearson correlation coefficient ( $r$ ) of GFP and mCherry fluorescence intensity (in arbitrary units, a.u.) along the nuclear rim of 30 cells, from three independent experiments. (C) Inhibiting NPC assembly reduces Heh2-IRC binding. Affinity purifications were performed from cell extracts derived from cells expressing Heh2-TAP with Nup192-FRB-GFP and Pma1-FKBP12 treated with carrier (DMSO) alone or with rapamycin (rap) to inhibit NPC assembly. Bound proteins were separated by SDS-PAGE and visualized with Coomassie. Positions of molecular weight markers (kilodaltons) are indicated at the left, and proteins are marked with colored circles that denote their identity as per the key at the right. Densitometry of the protein staining of the DMSO (black) and rapamycin (orange) lanes on the right. (D) Nup levels are not reduced upon inhibition of NPC assembly. Western blots using anti-GFP (top panel), anti-Pom152 (second panel), and anti-TAP (third panel) antibodies to detect the indicated proteins from whole-cell extracts derived from cells expressing Heh2-TAP (with Nup192-FRB-GFP and Pma1-FKBP12) treated with carrier (DMSO) or with rapamycin (rap). The fourth panel is a representative region of the nitrocellulose membrane stained with Ponceau S to evaluate total protein loads. Positions of molecular weight markers (kilodaltons) are indicated at the left.





reflect either too little (in the case of *heh2*-(1-570)) and likely inappropriate or untimely (in the case of *heh2*-(316-663)) interactions with nups.

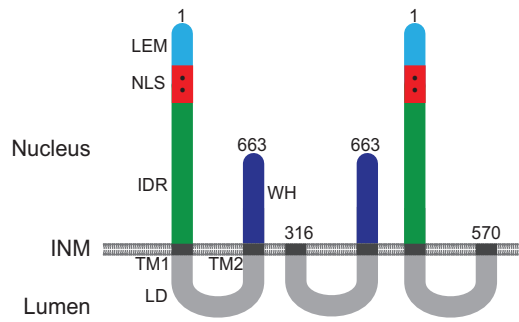
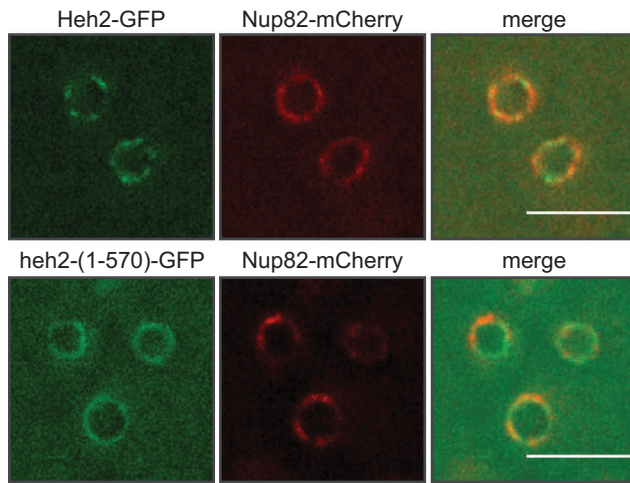
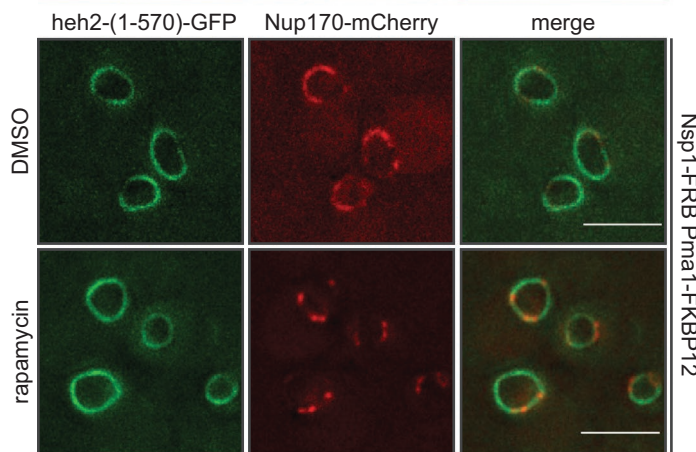
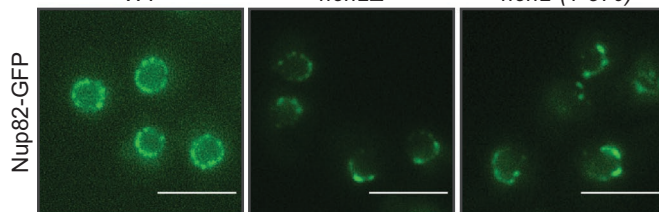
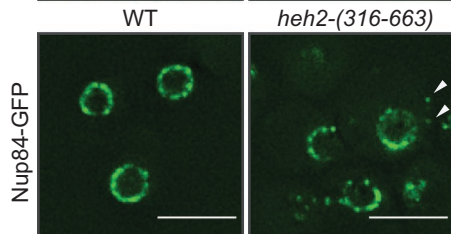
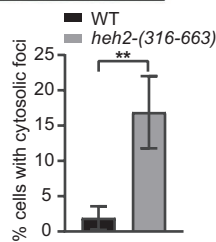
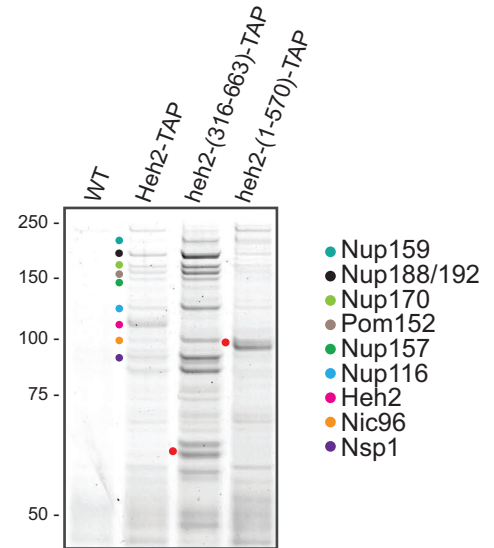
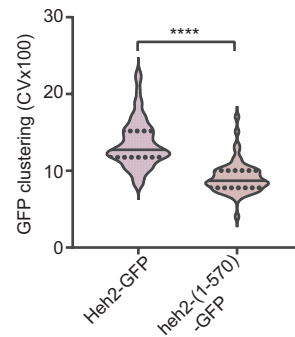
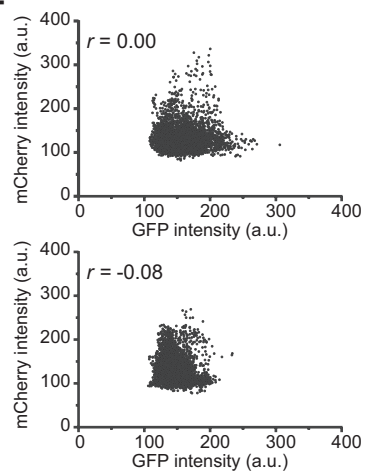
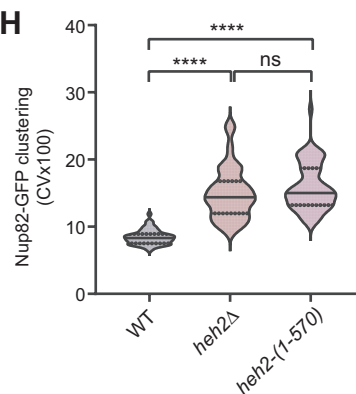
## DISCUSSION

We have explored the physical and functional relationship between the integral INM protein Heh2 and the NPC. This study was motivated by our prior discovery of predominantly genetic interactions between *HEH2* and *nup* genes (Yewdell *et al.*, 2011), in addition to other work considering Heh2 as a factor in a NPC assembly surveillance pathway (Webster *et al.*, 2014, 2016). In the latter, we suggested that Heh2 possesses the ability to discern between NPC assembly intermediates and fully formed NPCs. This concept was centered, in part, on data showing that Heh2 does not associate with clustered NPCs in *nup133Δ* strains (Figure 5), which was the premise for a model where Heh2 does not bind to fully formed NPCs. We now provide a more nuanced explanation for these data, as deletion of Nup133 (and other ORC nups) disrupts Heh2's otherwise robust physical association with the NPC (Figures 4A and 5). Thus, in light of the new data presented here, a reconsideration of the role of Heh2 in NPC biology is needed. Given these new observations, we suggest that Heh2 likely binds to fully formed NPCs. Several data support this assertion, including 1) the biochemical interactions that suggest the formation of a stable complex between Heh2 and the IRC (Figure 1, A and B); 2) the maintenance of these interactions even upon NPC assembly inhibition (Figure 3C); and 3) the punctate distribution of Heh2 at steady state and upon clustering of functional NPCs driven by the anchoring of Nsp1-FRB (Figure 2C) and in the strain carrying the *nup159-1* allele (Figure 5A).

Despite the demonstration that Heh2 associates with NPCs, several new conundrums arise as a consequence of this work. The first

**FIGURE 5:** Heh2's association with NPCs depends on the integrity of the NPC scaffold. (A) ORC gene knockouts reduce Heh2-GFP clustering at the nuclear envelope. Deconvolved fluorescence micrographs of Heh2-GFP and Nup82-mCherry with merge in WT and the indicated *nup* gene deletion or mutant strains. Arrowheads indicate regions devoid of Heh2-GFP where clustered NPCs are localized in *nup133Δ* cells. Scale bar is 5  $\mu$ m. (B) Heh2 does not enrich with NPC clusters in ORC deletion strains. Violin plot of the percent enrichment of Heh2-GFP within NPC clusters in individual cells with median (thick dotted lines) and quartiles (thin dotted lines) in the indicated *nup* gene deletion or mutant strains from three independent experiments (10 cells/strain per experiment). The width of the violins shows the frequency distribution of cells. *p* values were calculated with unpaired *t* test, where \*\*\*\* indicates  $p \leq 0.0001$ .

**FIGURE 4:** NPC scaffold integrity affects Heh2's association with NPCs. (A) Affinity purifications were performed from cell extracts derived from the indicated *nup* gene deletion strains expressing endogenous Heh2-TAP or from WT cells (no TAP). Bound proteins were separated by SDS-PAGE and visualized by Coomassie staining. Numbers at the left indicate positions of molecular weight standards in kilodaltons. Proteins are marked with colored circles that denote their identity as per the key at the right. Asterisks in the right panel indicate the position of a nonspecific protein that was affinity purified with a batch of IgG beads different from those used in the left panel affinity purifications. (B) The nups affinity purified from the indicated genetic backgrounds in A are placed within a single spoke of the NPC structure (from PDBDEV\_00000010; Kim *et al.*, 2018) in the side and center views. Individual nups are colored as in the key in A. Boxes in the *nup133Δ* model indicate positions where Nup133 would be located. (C) Deconvolved fluorescence micrographs of Heh2-GFP in the indicated strains. White arrowhead points to Heh2-GFP fluorescence at the cortical ER in *nup170Δ* cells. Scale bars are 5  $\mu$ m. (D) The distribution of Heh2-GFP at the nuclear envelope is unaltered in IRC deletion backgrounds. The CV of the GFP fluorescence along the nuclear envelope was calculated as a quantitative measure of Heh2-GFP clustering at the nuclear envelope. Individual CV values (multiplied by 100) were plotted with mean and SD from 60 cells from three independent experiments. The width of the violin shows the frequency distribution of cells; the thick and thin dotted lines specify the median and the quartiles, respectively. (E) As in A but affinity purifications performed from *S. pombe* cell extracts. Arrowheads point to the full-length and degradative forms of spHeh2-TAP.

**A****C****E****G****I****J****B****D****F****H**

is that we do not observe any robust physical association between Heh2 and the ORC, and yet, deletion of ORC nups, particularly Nup133, leads to a loss of Heh2 binding to the NPC (Figure 4A). In contrast, we cannot disrupt Heh2's association with NPCs by knocking out any individual component of the IRC (Figure 4, A and C). While the latter can be explained in a model where Heh2 makes several direct but redundant connections with nups, likely Pom152 and Nup170 and/or Nup188, the former is more challenging to interpret. Several potential models can be considered. The first deals with the very nature of *nup133Δ* NPC clustering, which has so far remained only partially explained on a mechanistic level. For example, one thought is that the association of NPCs with the pore membrane is destabilized without the amphipathic helix/ALPS motif in Nup133 (Drin *et al.*, 2007), which may lead to pore clustering (Fernandez-Martinez *et al.*, 2012). In such a scenario, given that it is an integral membrane protein, Heh2's interactions with the NPC may depend on the presence of specific lipids or membrane curvature (or both) at the pore membrane. It is also possible that the IRC may not be fully functional or be structurally perturbed in this context. Regardless of the underlying mechanism, as Heh2's association with the NPC ultimately depends on the function of both of its major scaffold complexes (i.e., the IRC and ORC), we favor a model in which Heh2 can, through a mechanism that remains to be defined, "sense" the structural integrity of the NPC.

A model in which Heh2 is a sensor for the NPC scaffold fits within a quality control mechanism framework. For example, recent work suggests that NPC clustering can facilitate clearance of NPCs by autophagy (Lee *et al.*, 2020). Thus, it is tempting to speculate that damage to the NPC scaffold may trigger the release of Heh2, which would in turn lead to the clustering of damaged NPCs. Such an idea is supported by the clustering that we observe in contexts where Heh2-NPC interactions are abrogated (Figure 6, G and H). Similarly, as we have previously reported, NPC clustering may also be an in-

put that ensures that damaged or malformed NPCs are not transmitted to daughter cells (Webster *et al.*, 2014). Thus, the consistent theme is that breaking interactions between Heh2 and NPCs may be an input to their segregation or clearance. A corollary to this is that Heh2 bound to NPCs may in fact promote the inheritance of functional NPCs. This may be best illustrated by work from *S. japonicus*, where it was demonstrated that the Heh2 orthologue contributes to anchoring NPCs to chromatin to promote their proper segregation between daughters (Yam *et al.*, 2013). Indeed, our observation that Heh2 also engaged in interactions with the IRC in *S. pombe* argues that it supports a fundamental role(s) across diverse yeasts.

How, then, do interactions between Heh2 and NPCs ensure proper NPC distribution? We speculate that in the absence of mechanisms to keep NPCs apart, NPCs have an inherent conformation or affinity that drives their clustering. In this scenario, tethering NPCs to INM proteins could help ensure their physical segregation. Although this could be envisaged as Heh2 acting as a physical buffer that prevents NPC–NPC interactions, we favor the concept that the distribution of NPCs and other elements of the nuclear architecture are codependent. Indeed, our prior work suggests that SpHeh2 antagonizes the flow of chromatin into nuclear deformations (Schreiner *et al.*, 2015), in essence maintaining normal chromatin distribution at the nuclear periphery, a direct corollary of the effect here on NPC distribution. As SpHeh2 binds both chromatin (Gonzalez *et al.*, 2012; Steglich *et al.*, 2012) and NPCs (this work), it is tempting to speculate that it supports the normal organization of NPCs and chromatin by dynamically linking these two major structural components of the nucleus. This concept is consistent with evidence in mammalian cells where NPCs are anchored to the lamin network (Daigle *et al.*, 2001; Maeshima *et al.*, 2006; Xie and Burke, 2017; Kittisopikul *et al.*, 2020). In scenarios in which this lamin connection is disrupted, for example, in lamin knockouts, NPCs also cluster

**FIGURE 6:** The WH domain of Heh2 is required for its association with NPCs. (A) Schematic of Heh2 and Heh2 truncations showing the LEM (Lap2-emerin-Man1) domain, a bipartite nuclear localization signal (NLS), intrinsically disordered region (IDR), luminal domain (LD), transmembrane domains (TM1 and TM2), and putative winged helix (WH); numbers represent amino acid numbers. INM, inner nuclear membrane. (B) Affinity purifications were performed from cell extracts derived from strains expressing the indicated TAP fusions or from WT cells (no TAP). Bound proteins were separated by SDS–PAGE and visualized by Coomassie staining. Proteins are marked with colored circles that denote their identity as per the key at the right. Numbers at the left indicate positions of molecular weight standards in kilodaltons. (C) Deconvolved fluorescence micrographs of Heh2-GFP or *heh2*-(1-570)-GFP and the NPC marker Nup82-mCherry, with merge. Scale bar is 5  $\mu$ m. (D) To quantitatively evaluate the distribution of Heh2-GFP and *heh2*-(1-570)-GFP, a CV of the GFP fluorescence along the nuclear envelope was calculated. Violin plots show the distribution of individual CV values (multiplied by 100) with median (solid line) and quartiles (dotted line) from 60 cells, from three independent experiments. The width of the violin specifies the frequency distribution of cells. *p* values were calculated from Student's *t* test, where \*\*\*\* indicates  $p \leq 0.0001$ . (E) Deconvolved fluorescence micrographs of *heh2*-(1-570)-GFP and Nup170-mCherry with merge in cells expressing Nsp1-FRB and Pma1-FKBP12. Cells were treated with carrier (DMSO) or rapamycin. Addition of rapamycin leads to NPC clustering as described in Figure 2A. Scale bar is 5  $\mu$ m. (F) Scatterplot with Pearson correlation coefficient (*r*) of *heh2*-(1-570)-GFP and Nup170-mCherry fluorescence intensity (in arbitrary units, a.u.) along the nuclear envelope of 30 cells from three independent experiments like that shown in E. Values are from cells from DMSO (top) and rapamycin-treated (bottom) conditions. (G) The WH domain of Heh2 is required for normal NPC distribution. Deconvolved fluorescence micrographs of Nup82-GFP in the indicated strain backgrounds. Scale bar is 5  $\mu$ m. (H) To quantitatively evaluate the distribution of Nup82-GFP in the indicated strains, a CV of the GFP fluorescence along the nuclear envelope was calculated. Violin plots show the distribution of individual CV values (multiplied by 100) with median (solid line) and quartiles (dotted line) from 60 cells, from three independent experiments. The width of the violin specifies the frequency distribution of cells. *p* values were calculated from one-way analysis of variance with Tukey's post-hoc test, where ns is  $p > 0.05$ , \*\*\*\* $p \leq 0.0001$ . (I) Deconvolved fluorescence micrographs of Nup84-GFP in WT and cells where *HEH2* is replaced by *heh2*-(316-663). Arrowheads point to cytosolic Nup84-GFP foci. Scale bar is 5  $\mu$ m. (J) Plot of the percentage of cells where Nup84-GFP is found in the cytosol from experiment in I. Error bars are SD from four independent experiments where more than 500 total cells were counted for each. *p* values were calculated with unpaired *t* test, where \*\* indicates  $p \leq 0.01$ .

together (Xie and Burke, 2017; Kittisopikul et al., 2020). Although NPCs are more dynamic along the nuclear envelope in budding yeast than in lamin-containing cells (Belgareh and Doye, 1997; Bucci and Wentz, 1997), their interactions with chromatin through multiple mechanisms (Luthra et al., 2007; Tan-Wong et al., 2009) could nonetheless contribute to their normal distribution. Whether clustering has an impact on NPC function per se remains ill-defined, although one could speculate that NPC clustering has a more profound impact on the NPC's roles in chromatin organization and gene expression as opposed to nuclear transport (Capelson et al., 2010; Raices and D'Angelo, 2017).

One particularly interesting feature of our analysis of Heh2 is that the NPC interaction and INM targeting sequences are distinct and on two physically separated domains. Certainly there is evidence from both genetic and biochemical analyses where the function of specific domains of the LEM domain proteins can be separated (Grund et al., 2008; Yewdell et al., 2011; Barrales et al., 2016; Hirano et al., 2018; Thaller et al., 2019; von Appen et al., 2020). However, we wonder whether there are functional implications for the integration of these two interaction platforms, which could place Heh2 in a tug-of-war between its residence bound to the NPC and its release to the INM. This would be yet another example in an emerging theme for these LEM domain proteins in which they bridge distinct sets of physical interactions to maintain the dynamic organization of the nuclear envelope system.

## MATERIALS AND METHODS

### Yeast culture and strain generation

All yeast strains used in this study are listed in Supplemental Table S2. *S. cerevisiae* strains were grown in YPD consisting of 1% yeast extract (BD), 2% bacto-peptone (BD), and 2% D-glucose (Sigma). For microscopy experiments, YPD was supplemented with 0.025% adenine hemisulfate (Sigma). Yeast cells were grown at 30°C to mid-log phase, unless otherwise stated. Transformation of *S. cerevisiae* cells, mating, sporulation, and tetrad dissections were carried out using standard protocols (Amberg et al., 2005). Deletion and truncation of yeast open reading frames (ORF) and tagging of ORFs with fluorescent protein genes, FRB, and TAP-tags were performed utilizing the pFA6a or pK3F plasmid templates (Longtine et al., 1998; Zhang et al., 2017).

*S. pombe* strains were grown in YE5S media consisting of 5% yeast extract (BD), 30% D-glucose (Sigma), and 1.25% SP complete supplements (adenine hemisulfate, L-histidine hydrochloride monohydrate, L-leucine, L-lysine hydrochloride, and uracil) from Sunrise Science products, at 30°C. *S. pombe* strains were crossed and maintained utilizing standard media and techniques as described in Moreno et al. (1991). PCR-based gene disruption and tagging were performed utilizing pFA6a plasmid templates (Bähler et al., 1998; Hentges et al., 2005).

### Plasmids

All plasmids used in this study are listed in Supplemental Table S2. The pFA6a-TAP-his3MX6 and pFA6a-TAP-TRP1 plasmids were constructed as follows: the TAP coding sequence was PCR-amplified from chromosomal DNA from a strain expressing Heh2-TAP (SB-CPL42; Dharmacon yeast resources) using Phusion High fidelity DNA polymerase (New England BioLabs) and cloned into the *PacI* and *Ascl* sites of pFA6a-his3MX6 and pFA6a-TRP1.

pFA6a-3xHA-FRB-GFP-his3MX6 was generated by Gibson Assembly (New England BioLabs). The 3xHA epitope coding sequence was PCR-amplified from pFA6a-3xHA-hisMX6 (Longtine et al., 1998) using Q5 DNA polymerase (New England BioLabs) and assembled

into pFA6a-FRB-GFP-hisMX6, or pFA6a-FRB-hisMX6 (EUROSCARF) digested with *Sall* and *PacI*.

### Conjugation of Dynabeads with rabbit IgG

Purified rabbit immunoglobulin G (IgG) (Sigma; I5006) was dissolved in 0.1 M sodium phosphate buffer, pH 7.4, to a final concentration of 1 mg/ml. The IgG solution was filtered through a 0.22 µm syringe filter and mixed with an equal volume of 3 M (NH<sub>4</sub>)<sub>2</sub>SO<sub>4</sub>. For conjugation, Dynabeads M-270 Epoxy (Invitrogen; 100 mg) were transferred to a 15 ml centrifuge tube, suspended in 6 ml 0.1 M sodium phosphate buffer, pH 7.4, and incubated at room temperature for 15 min on a tube rotator. The beads were collected on a magnetic rack, the buffer aspirated, and the beads were washed again with 0.1 M sodium phosphate buffer, pH 7.4, by vortexing. The buffer was removed, and beads were resuspended in 2 ml of IgG solution and incubated at 30°C for 65–70 h on a tube rotator. The beads were separated on a magnetic rack and quickly washed with 100 mM glycine, pH 2.5, followed by a wash with 10 mM Tris-HCl, pH 8.8. The beads were again washed quickly with freshly prepared 100 mM triethylamine followed by four washes with phosphate-buffered saline (PBS) for 5 min each and one wash with PBS with 0.5% Triton X-100 for 15 min. The beads were washed one final time with PBS, collected on a magnetic rack, and resuspended in 667 µl PBS with 50% glycerol.

### Immunoaffinity purification

To affinity purify TAP-fusions, *S. cerevisiae* strains were grown overnight and 2 ml of culture was diluted into 1 l of YPD the next morning and grown for 20–24 h to late log phase (OD<sub>600</sub> ~ 2). *S. pombe* cells were grown overnight and transferred to fresh medium the next morning to an OD<sub>600</sub> of 0.1 and grown for 7 h. *S. pombe* cells were further diluted to an OD<sub>600</sub> of 0.01 in 1 l YES medium and grown for another 18–20 h. Both *S. cerevisiae* and *S. pombe* cells were grown at 30°C at 200 rpm, and cells were harvested by centrifugation. Cells were washed with ice-cold water once, collected by centrifugation, and resuspended in 100 µl of freezing solution (20 mM HEPES, pH 7.4, 1.2% polyvinylpyrrolidone, and protease inhibitor cocktail [Sigma]) per g of cells. The cell slurry was snap-frozen in liquid nitrogen immediately. The frozen cell pellets were cryomilled six times at 30 Hz for 3 min in a Retsch MM400 mixer mill and stored at –80°C.

To perform immunoaffinity purifications, 200 mg of frozen yeast grindate was resuspended in a 4x volume of homogenization buffer (400 mM Na<sub>3</sub>Cit, pH 8.0, 10 mM Deoxy Big CHAP) and protease inhibitor cocktail at room temperature. The homogenate was clarified by centrifugation at 16,000 × g for 10 min at 4°C. The soluble fraction was incubated with 25 µl of rabbit-IgG-coated Dynabeads for 1 h at 4°C under gentle rotation. After binding, beads were collected on a magnetic rack and washed three times with 500 µl ice-cold homogenization buffer. The proteins were eluted by incubating beads with 20 µl of 1x NuPAGE lithium dodecyl sulfate sample buffer (Invitrogen) at room temperature for 10 min. The eluate was separated on a magnetic rack and further incubated with 50 mM dithiothreitol at 70°C for 10 min. The eluted proteins were separated on a 4–12% NuPAGE gel (Novex) and stained with Imperial protein stain (Thermo Scientific). The proteins of interest were excised for identification by MS.

### Mass spectrometry

Excised SDS-PAGE gel pieces were washed with deionized water and transferred to a 1.5 ml tube, and in-gel tryptic digestion was performed. The peptides were separated on a Waters nanoACQUITY ultra-high-pressure liquid chromatograph and detected on a

ThermoFisher Q Executive mass spectrometer. The MS/MS data were analyzed by the Mascot software (Matrix Science, London, UK; version 2.6.1) to search the SwissProt\_2019\_08.fasta tax:Schizosaccharomyces pombe or SwissProt\_2018\_10.fasta tax:Saccharomyces cerevisiae database. Mascot search parameters allowed variable modifications (oxidation [M], carbamidomethyl [C], propionamide [C]), a peptide mass tolerance of 10 ppm, and a fragment ion mass tolerance of 0.02 Da. The total score assigned by Mascot search is the probability of the observed match to be a random event, and expectation values represent the number of protein matches with equal or better scores than are expected to occur by chance alone. emPAI (exponentially modified protein abundance index) is the approximate, relative quantification of the protein in a mixture as described by Ishihama et al. (2005).

### Anchor Away experiments

The Anchor Away experiments were performed as described by Haurki et al. (2008). Briefly, strains expressing Nup-FRB fusions and Pma1-FKPB12 in HHY110 (*tor1-1 fpr1Δ*) were incubated with a final concentration of 1 μg/ml rapamycin for 30 min (to cluster NPCs in the context of Nsp1-FRB) or 3 h to inhibit assembly (Nup192-FRB).

### Western blotting

To visualize protein levels by Western blotting, whole-cell protein extracts were prepared from 2 OD<sub>600</sub> cells. Cells were washed once with 1 mM EDTA and lysed by resuspension in 2 N NaOH for 10 min on ice. To precipitate the proteins, the cell lysate was incubated with 50% trichloroacetic acid for 20 min on ice and collected by centrifugation. The protein precipitate was washed with ice-cold acetone, air-dried at room temperature, and resuspended in SDS-PAGE sample buffer. The protein samples were denatured at 95°C for 5 min and separated on a 4–12% SDS-PAGE gradient gel (Bio-Rad). The proteins were transferred to a 0.2 μm nitrocellulose membrane. To ensure equal protein loading across samples, the nitrocellulose membrane was stained with Ponceau S solution (Sigma). The membranes were washed once with tris-buffered saline-tween (TBST: 20 mM Tris-Cl, pH 7.5, 150 mM NaCl, 0.1% Tween 20) and blocked with 5% nonfat dry milk powder (Sigma) in TBST for 1 h. The blocked membranes were incubated with primary antibodies: anti-TAP (CAB1001; Thermo Fisher Scientific), anti-GFP (rabbit polyclonal), and anti-Pom152 (rabbit polyclonal, raised against a peptide in the Pom152 luminal domain) for 1 h at room temperature. The primary antibodies were detected with anti-rabbit horseradish peroxidase-conjugated secondary antibodies and visualized with the Pierce ECL Western blotting substrate (Thermo Fisher Scientific) in a Versadoc Imaging System (Bio-Rad).

### Fluorescence microscopy, image processing, and analysis

Fluorescence micrographs were acquired on a DeltaVision microscope (Applied Precision, GE Healthcare) with a 100x, 1.4 NA objective (Olympus). The images were captured with a CoolSnapHQ<sup>2</sup> CCD camera (Photometrics). Fluorescence micrographs were deconvolved with the iterative algorithm sofWoRx 6.5.1 (Applied Precision, GE Healthcare).

Clustering of NPCs was quantified as described previously (Fernandez-Martinez et al., 2012): A 6-pixel-wide freehand line was drawn along the nuclear envelope contour, and mean fluorescence intensities were measured using FIJI/ImageJ (Schindelin et al., 2012). Clustering was assessed by calculating the CV (SD/mean × 100) of the fluorescence intensities at the nuclear envelope.

To measure the enrichment of Heh2 at the NPC clusters in nup deleted or mutant strains, the raw integrated density of the GFP

signal at the NPC clusters and along the entire nuclear envelope was measured utilizing FIJI/ImageJ (Schindelin et al., 2012). The fraction of signal density at the NPC clusters was calculated out of the total signal density to yield the percent Heh2-GFP enrichment.

### Modeling of NPC spokes

Color coding of an isosurface representation of individual nup densities as assigned in Kim et al. (2018) within an individual spoke of the NPC from the PDB DEV ID:00000010 was completed using ChimeraX (UCSF) (Goddard et al., 2018).

### ACKNOWLEDGMENTS

We thank Jean Kanyo and the Yale Keck Biotechnology Resource Laboratory for help with MS analysis. We thank Valérie Doye for *S. pombe* strains. We thank the members of the LusKing laboratory for critical input on experimental design and data analysis. This work was supported by the National Institutes of Health: R01 GM105672 to C.P.L. and R01 GM112108 and P41 GM109824 to M.P.R.; and the National Science Foundation: EFMA-1806504 to M.C.K.

### REFERENCES

- Amberg DC, Burke DJ, Strathern JN (2005). *Methods in Yeast Genetics: A Cold Spring Harbor Laboratory Course Manual*, 2005 ed., Cold Spring Harbor, NY: Cold Spring Harbor Laboratory Press.
- Asakawa H, Kojidani T, Yang HJ, Ohtsuki C, Osakada H, Matsuda A, Iwamoto M, Chikashige Y, Nagao K, Obuse C, et al. (2019). Asymmetrical localization of nup107-160 subcomplex components within the nuclear pore complex in fission yeast. *PLoS Genet* 15, 1–30.
- Asakawa H, Yang HJ, Yamamoto TG, Ohtsuki C, Chikashige Y, Sakata-Sogawa K, Tokunaga M, Iwamoto M, Hiraoka Y, Haraguchi T (2014). Characterization of nuclear pore complex components in fission yeast *Schizosaccharomyces pombe*. *Nucleus* 5, 149–162.
- Bähler J, Wu JQ, Longtine MS, Shah NG, McKenzie A, Steever AB, Wach A, Philippsen P, Pringle JR (1998). Heterologous modules for efficient and versatile PCR-based gene targeting in *Schizosaccharomyces pombe*. *Yeast* 14, 943–951.
- Bai SW, Rouquette J, Umeda M, Faigle W, Loew D, Sazer S, Doye V (2004). The fission yeast Nup107-120 complex functionally interacts with the small GTPase Ran/Spi1 and is required for mRNA export, nuclear pore distribution, and proper cell division. *Mol Cell Biol* 24, 6379–6392.
- Barrales RR, Forn M, Georgescu PR, Sarkadi Z, Braun S (2016). Control of heterochromatin localization and silencing by the nuclear membrane protein Lem2. *Genes Dev* 30, 133–148.
- Barton LJ, Soshnev AA, Geyer PK (2015). Networking in the nucleus: a spotlight on LEM-domain proteins. *Curr Opin Cell Biol* 34, 1–8.
- Belgareh N, Doye V (1997). Dynamics of nuclear pore distribution in nucleoporin mutant yeast cells. *J Cell Biol* 136, 747–759.
- Bucci M, Wentz SR (1997). In vivo dynamics of nuclear pore complexes in yeast. *J Cell Biol* 136, 1185–1199.
- Buchwalter A, Kaneshiro JM, Hetzer MW (2019). Coaching from the sidelines: the nuclear periphery in genome regulation. *Nat Rev Genet* 20, 39–50.
- Burke B, Roux KJ (2009). Nuclei take a position: managing nuclear location. *Dev Cell* 17, 587–597.
- Cai M, Huang Y, Suh J-Y, Louis JM, Ghirlando R, Craigie R, Clore GM (2007). Solution NMR structure of the barrier-to-autointegration factor-Emerin complex. *J Biol Chem* 282, 14525–14535.
- Capelson M, Doucet C, Hetzer MW (2010). Nuclear pore complexes: guardians of the nuclear genome. *Cold Spring Harb Symp Quant Biol* 75, 585–597.
- Caputo S, Couprie J, Duband-Goulet I, Kondé E, Lin F, Braud S, Gondry M, Gilquin B, Worman HJ, Zinn-Justin S (2006). The carboxyl-terminal nucleoplasmic region of MAN1 exhibits a DNA binding winged helix domain. *J Biol Chem* 281, 18208–18215.
- Chen XQ, Du X, Liu J, Balasubramanian MK, Balasundaram D (2004). Identification of genes encoding putative nucleoporins and transport factors in the fission yeast *Schizosaccharomyces pombe*: a deletion analysis. *Yeast* 21, 495–509.
- Colombi P, Webster BM, Fröhlich F, Lusk CP (2013). The transmission of nuclear pore complexes to daughter cells requires a cytoplasmic pool of Nsp1. *J Cell Biol* 203, 215–232.

- Daigle N, Beaudouin J, Hartnell L, Imreh G, Hallberg E, Lippincott-Schwartz J, Ellenberg J (2001). Nuclear pore complexes form immobile networks and have a very low turnover in live mammalian cells. *J Cell Biol* 154, 71–84.
- Doye V, Wepf R, Hurt EC (1994). A novel nuclear pore protein Nup133p with distinct roles in poly(A)<sup>+</sup> RNA transport and nuclear pore distribution. *EMBO J* 13, 6062–6075.
- Drin G, Casella JF, Gautier R, Boehmer T, Schwartz TU, Antonny B (2007). A general amphipathic  $\alpha$ -helical motif for sensing membrane curvature. *Nat Struct Mol Biol* 14, 138–146.
- Fernandez-Martinez J, Phillips J, Sekedat MD, Diaz-Avalos R, Velazquez-Muriel J, Franke JD, Williams R, Stokes DL, Chait BT, Sali A, Rout MP (2012). Structure-function mapping of a heptameric module in the nuclear pore complex. *J Cell Biol* 196, 419–434.
- Fernandez-Martinez J, Rout MP (2021). One ring to rule them all? Structural and functional diversity in the nuclear pore complex. *Trends Biochem Sci*, doi: 10.1016/j.tibs.2021.01.003.
- Furukawa K (1999). LAP2 binding protein 1 (L2BP1/BAF) is a candidate mediator of LAP2-chromatin interaction. *J Cell Sci* 112, 2485–2492.
- Goddard TD, Huang CC, Meng EC, Pettersen EF, Couch GS, Morris JH, Ferrin TE (2018). UCSF ChimeraX: meeting modern challenges in visualization and analysis. *Protein Sci* 27, 14–25.
- Gonzalez Y, Saito A, Sazer S (2012). Fission yeast Lem2 and Man1 perform fundamental functions of the animal cell nuclear lamina. *Nucleus* 3, 60–76.
- Gorsch LC, Dockendorff TC, Cole CN (1995). A conditional allele of the novel repeat-containing yeast nucleoporin RAT7/NUP159 causes both rapid cessation of mRNA export and reversible clustering of nuclear pore complexes. *J Cell Biol* 129, 939–955.
- Grund SE, Fischer T, Cabal GG, Antúñez O, Pérez-Ortín JE, Hurt E (2008). The inner nuclear membrane protein Src1 associates with subtelomeric genes and alters their regulated gene expression. *J Cell Biol* 182, 897–910.
- Hakhverdyan Z, Domanski M, Hough LE, Oroskar ARAA, Oroskar ARAA, Keegan S, Dilworth DJ, Molloy KR, Sherman V, Aitchison JD, et al. (2015). Rapid, optimized interactomic screening. *Nat Methods* 12, 553–560.
- Hampoeiz B, Andres-Pons A, Kastiris P, Beck M (2019). Structure and assembly of the nuclear pore complex. *Annu Rev Biophys* 48, 515–536.
- Haruki H, Nishikawa J, Laemmler UK (2008). The Anchor-Away technique: rapid, conditional establishment of yeast mutant phenotypes. *Mol Cell* 31, 925–932.
- Hentges P, Van Driessche B, Tafforeau L, Vandenhaute J, Carr AM (2005). Three novel antibiotic marker cassettes for gene disruption and marker switching in *Schizosaccharomyces pombe*. *Yeast* 22, 1013–1019.
- Hirano Y, Kinugasa Y, Asakawa H, Chikashige Y, Obuse C, Haraguchi T, Hiraoka Y (2018). Lem2 is retained at the nuclear envelope through its interaction with Bqt4 in fission yeast. *Genes Cells* 23, 122–135.
- Ishihama Y, Oda Y, Tabata T, Sato T, Nagasu T, Rappsilber J, Mann M (2005). Exponentially modified protein abundance index (emPAI) for estimation of absolute protein amount in proteomics by the number of sequenced peptides per protein. *Mol Cell Proteomics* 4, 1265–1272.
- Kim SJ, Fernandez-Martinez J, Nudelman I, Shi Y, Zhang W, Raveh B, Herricks T, Slaughter BD, Hogan JA, Upla P, et al. (2018). Integrative structure and functional anatomy of a nuclear pore complex. *Nature* 555, 475–482.
- King MC, Lusk CP, Blobel G (2006). Karyopherin-mediated import of integral inner nuclear membrane proteins. *Nature* 442, 1003–1007.
- Kittisopikul M, Shimi T, Tatli M, Tran JR, Zheng Y, Medalia O, Jaqaman K, Adam SA, Goldman RD (2020). Computational analyses reveal spatial relationships between nuclear pore complexes and specific lamins. *J Cell Biol* 220, e202007082.
- Kosinski J, Mosalaganti S, von Appen A, Teimer R, DiGuilio AL, Wan W, Bui KH, Hagen WJH, Briggs JAG, Glavy JS, et al. (2016). Molecular architecture of the inner ring scaffold of the human nuclear pore complex. *Science* 352, 363–365.
- Lee CW, Wilfling F, Ronchi P, Allegretti M, Mosalaganti S, Jentsch S, Beck M, Pfander B (2020). Selective autophagy degrades nuclear pore complexes. *Nat Cell Biol* 22, 159–166.
- Longtine MS, McKenzie A, Demarini DJ, Shah NG, Wach A, Brachat A, Philippsen P, Pringle JR (1998). Additional modules for versatile and economical PCR-based gene deletion and modification in *Saccharomyces cerevisiae*. *Yeast* 14, 953–961.
- Luthra R, Kerr SC, Harreman MT, Apponi LH, Fasken MB, Ramineni S, Chaurasia S, Valentini SR, Corbett AH (2007). Actively transcribed GAL genes can be physically linked to the nuclear pore by the SAGA chromatin modifying complex. *J Biol Chem* 282, 3042–3049.
- Maeshima K, Yahata K, Sasaki Y, Nakatomi R, Tachibana T, Hashikawa T, Imamoto F, Imamoto N (2006). Cell-cycle-dependent dynamics of nuclear pores: pore-free islands and lamins. *J Cell Sci* 119, 4442–4451.
- Makio T, Stanton LH, Lin CC, Goldfarb DS, Weis K, Wozniak RW (2009). The nucleoporins Nup170p and Nup157p are essential for nuclear pore complex assembly. *J Cell Biol* 185, 459–473.
- Mans BJ, Anantharaman V, Aravind L, Koonin EV (2004). Comparative genomics, evolution and origins of the nuclear envelope and nuclear pore complex. *Cell Cycle* 3, 1625–1650.
- Marelli M, Lusk CP, Chan H, Aitchison JD, Wozniak RW (2001). A link between the synthesis of nucleoporins and the biogenesis of the nuclear envelope. *J Cell Biol* 153, 709–724.
- Meinema AC, Laba JK, Hapsari RA, Otten R, Mulder FAA, Kralt A, Van Den Bogaart G, Lusk CP, Poolman B, Veenhoff LM (2011). Long unfolded linkers facilitate membrane protein import through the nuclear pore complex. *Science* (80 333), 90–93.
- Mekhail K, Moazed D (2010). The nuclear envelope in genome organization, expression and stability. *Nat Rev Mol Cell Biol* 11, 317–328.
- Mekhail K, Seebacher J, Gygi SP, Moazed D (2008). Role for perinuclear chromosome tethering in maintenance of genome stability. *Nature* 456, 667–670.
- Mészáros N, Cibulka J, Mendiburo MJ, Romanauska A, Schneider M, Köhler A (2015). Nuclear pore basket proteins are tethered to the nuclear envelope and can regulate membrane curvature. *Dev Cell* 33, 285–298.
- Moreno S, Klar A, Nurse P (1991). Molecular genetic analysis of fission yeast *Schizosaccharomyces pombe*. *Methods Enzymol* 194, 795–823.
- Onischenko E, Tang JH, Andersen KR, Knockenhauer KE, Vallotton P, Derrer CP, Kralt A, Mugler CF, Chan LY, Schwartz TU, Weis K (2017). Natively unfolded FG repeats stabilize the structure of the nuclear pore complex. *Cell* 171, 904–917.e19.
- Otsuka S, Bui KH, Schorb M, Hossain MJ, Politi AZ, Koch B, Eltsov M, Beck M, Ellenberg J (2016). Nuclear pore assembly proceeds by an inside-out extrusion of the nuclear envelope. *eLife* 5, 1–23.
- Pemberton LF, Rout MP, Blobel G (1995). Disruption of the nucleoporin gene NUP133 results in clustering of nuclear pore complexes. *Proc Natl Acad Sci USA* 92, 1187–1191.
- Raices M, D'Angelo MA (2017). Nuclear pore complexes and regulation of gene expression. *Curr Opin Cell Biol* 46, 26–32.
- Rhind N, Chen Z, Yassour M, Thompson DA, Haas BJ, Habib N, Wapinski I, Roy S, Lin MF, Heiman DI, et al. (2011). Comparative functional genomics of the fission yeasts. *Science* 332, 930–936.
- Schindelin J, Arganda-Carreras I, Frise E, Kaynig V, Longair M, Pietzsch T, Preibisch S, Rueden C, Saalfeld S, Schmid B, et al. (2012). Fiji: an open-source platform for biological-image analysis. *Nat Methods* 9, 676–682.
- Schreiner SM, Koo PK, Zhao Y, Mochrie SGJ, King MC (2015). The tethering of chromatin to the nuclear envelope supports nuclear mechanics. *Nat Commun* 6, 1–13.
- Steglich B, Filion GJ, van Steensel B, Ekwall K (2012). The inner nuclear membrane proteins Man1 and Ima1 link to two different types of chromatin at the nuclear periphery in *S. pombe*. *Nucleus* 3, 77–87.
- Taddei A, Gasser SM (2012). Structure and function in the budding yeast nucleus. *Genetics* 192, 107–129.
- Tan-Wong SM, Wijayatilake HD, Proudfoot NJ (2009). Gene loops function to maintain transcriptional memory through interaction with the nuclear pore complex. *Genes Dev* 23, 2610–2624.
- Thaller DJ, Allegretti M, Borah S, Ronchi P, Beck M, Lusk CP (2019). An ESCRT-LEM protein surveillance system is poised to directly monitor the nuclear envelope and nuclear transport system. *eLife* 8, e45284.
- Thaller DJ, Lusk CP (2018). Fantastic nuclear envelope herniations and where to find them. *Biochem Soc Trans* 46, 877–889.
- Thaller DJ, Tong D, Marklew CJ, Ader NR, Mannino PJ, Borah S, King MC, Ciani B, Lusk CP (2021). Direct binding of ESCRT protein Chm7 to phosphatidic acid-rich membranes at nuclear envelope herniations. *J Cell Biol* 220, jcb.202004222.
- Ungricht R, Kutay U (2015). Establishment of NE asymmetry—targeting of membrane proteins to the inner nuclear membrane. *Curr Opin Cell Biol* 34, 135–141.
- Ungricht R, Kutay U (2017). Mechanisms and functions of nuclear envelope remodelling. *Nat Rev Mol Cell Biol* 18, 229–245.
- von Appen A, LaJoie D, Johnson IE, Trnka MJ, Pick SM, Burlingame AL, Ullman KS, Frost A (2020). LEM2 phase separation promotes ESCRT-mediated nuclear envelope reformation. *Nature* 582, 115–118.
- Webster BM, Colombi P, Jäger J, Lusk CP (2014). Surveillance of nuclear pore complex assembly by ESCRT-III/Vps4. *Cell* 159, 388–401.

- Webster BM, Thaller DJ, Jäger J, Ochmann SE, Borah S, Lusk CP (2016). Chm7 and Heh1 collaborate to link nuclear pore complex quality control with nuclear envelope sealing. *EMBO J* 35, 2447–2467.
- Xie W, Burke B (2017). Nuclear networking. *Nucleus* 8, 323–330.
- Yam C, Gu Y, Oliferenko S (2013). Partitioning and remodeling of the *Schizosaccharomyces japonicus* mitotic nucleus require chromosome tethers. *Curr Biol* 23, 2303–2310.
- Yewdell WT, Colombi P, Makhnevych T, Lusk CP (2011). Luminal interactions in nuclear pore complex assembly and stability. *Mol Biol Cell* 22, 1375–1388.
- Zhang Y, Serratore ND, Briggs SD (2017). N-ICE plasmids for generating N-terminal 3 × FLAG tagged genes that allow inducible, constitutive or endogenous expression in *Saccharomyces cerevisiae*. *Yeast* 34, 223–235.